



HAL
open science

Benchmark for fluid flow in weld pool simulation : two-dimensional transient computational models for arc welding

Pascal Girard, Michel Bellet, Georges Caillibotte, M. Carin, Stephane Gounand, François Mathey, Marc Medale

► To cite this version:

Pascal Girard, Michel Bellet, Georges Caillibotte, M. Carin, Stephane Gounand, et al.. Benchmark for fluid flow in weld pool simulation : two-dimensional transient computational models for arc welding. 2005. hal-04108230

HAL Id: hal-04108230

<https://hal.science/hal-04108230>

Preprint submitted on 1 Jun 2023

HAL is a multi-disciplinary open access archive for the deposit and dissemination of scientific research documents, whether they are published or not. The documents may come from teaching and research institutions in France or abroad, or from public or private research centers.

L'archive ouverte pluridisciplinaire **HAL**, est destinée au dépôt et à la diffusion de documents scientifiques de niveau recherche, publiés ou non, émanant des établissements d'enseignement et de recherche français ou étrangers, des laboratoires publics ou privés.



Distributed under a Creative Commons Attribution - NonCommercial 4.0 International License

Benchmark for fluid flow in weld pool simulation

Two-dimensional transient computational models for arc welding

P. Girard, M. Bellet G. Caillibotte, M. Carin, S. Gounand, F. Mathey
and M. Médale

Abstract: A numerical benchmark for the weld pool simulation is presented for a case representative of a spot GTA welding. It has been treated by five institutes or industrial companies with five computational fluid dynamics codes (CFD). Comparative results are presented for a transient spot welding simulation on a 304L-Like material. Four observables (temperature and velocity) are studied on a transient duration of 5 s. A good agreement is shown between all CFD codes Relevant observables allowing to discriminate models are exhibited. Remaining discrepancies are discussed.

Keywords : weld pool simulation, numerical benchmark, arc welding transient models, thermocapillary, fluid dynamics.

P. Girard (pascal.girard@cea.fr) CEA-Saclay (UTIAC/LMAP) 91191 Gif sur Yvette cedex France, M. Bellet (michel.ballet@ensmp.fr) Ecole des Mines de Paris – Centre de Mise en forme des matériaux, BP 207, 06904 Sophia Antipolis, France, G. Caillibotte (georges.caillibotte@airliquide.com) Air Liquide CRCD 1, Chemin de la porte des loges - Les loges en Josas BP 126 - 78 354 Jouy en Josas Cedex France, M Carin (marcel.carin@univ-ubs.fr) Laboratoire d'Etudes Thermiques Energétiques et Environnement, Université de Bretagne Sud Rue de Saint Maudé 56321 Lorient cedex France, S. Gounand (gounand@sem2.smts.cea.fr) CEA-Saclay (SFME/LTMF) 91191 Gif sur Yvette cedex France, F. Mathey (fabricem@fluent.fr) 1, place Charles de Gaulle Immeuble Central Gare 78180 Montigny le Bretonneux France and M. Médale (Marc.Medale@polytech.univ-mrs.fr) Ecole Polytechnique Universitaire de Marseille, UMR 6595, Université de Provence, Technopôle de Château-Gombert, 5 rue Enrico-Fermi, 13453 Marseille Cedex 13 France.

INTRODUCTION

The continuous activity of the last decades^(1,2) in numerical simulation of the weld-pool has allowed to increase the complexity of the physical mechanisms taken into account⁽³⁾. Outcomes have consisted in simulation of surface deformation, surface tension gradient⁽⁴⁾ and Lorentz forces⁽⁵⁾. Numerical methods have been developed and tested as well⁽⁶⁾.

The state of the art allows us to investigate the process to part coupling^(7,8) through more and more accurate description of the boundary conditions.

However, reflecting the approaches diversity, results and simulation models are hardly comparable due to the different model ingredients and boundary conditions choice. Moreover coupled physics processes prevent to reach an experimental validation of a particular effect description. The complexity of simulations and methods is then counterbalanced by the lack of references or validations. Reference data are needed in order to compare different simulation methods, CFD codes and increase weld-pool simulation reliability.

In this framework, several French teams, research centers and industrial companies, within a collaboration program, settled a standard benchmark which has been defined with a low complexity allowing a large range of contributors.

This benchmark aims to give reference data for a simple case representative of welding simulation.

It represents the first seconds of material melting, as occurring during spot GTAW on a disc.

This benchmark has been carried out with five CFD codes:

- FLUENT (Air Liquide and Fluent France⁹)
- FEMLAB⁽¹⁰⁾ (University of Bretagne Sud)
- MARCUS⁽¹¹⁻¹⁴⁾ (University of Provence)
- CASTEM⁽¹⁵⁾ (CEA – Saclay)
- THERCAST⁽¹⁷⁻²⁰⁾ (Ecole des Mines de Paris, CEMEF).

BENCHMARK DEFINITION

The benchmark represents the simulation of a spot GTAW with simple material models (fig. 1) :

The dimensions of the disc are: $3 \cdot 10^{-2}$ m radius and $1 \cdot 10^{-2}$ m thickness with an initial temperature of 300 K.

General assumptions:

- The system is 2-dimensional axisymmetric.
- The melted material is isotropic, homogeneous and incompressible (except buoyancy) and Newtonian.
- $|g| = 9.81 \text{ m s}^{-2}$.
- The flow is laminar.
- The weld pool surface is flat.

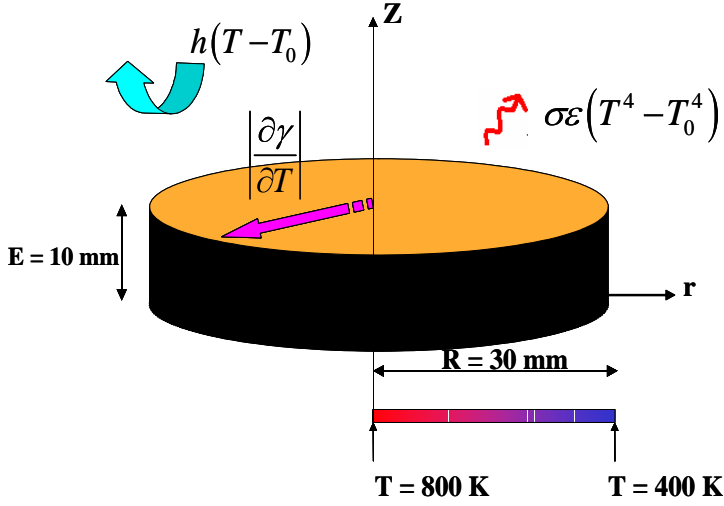


Fig. 1: Schematic illustration of the part and boundary conditions.

The material of concern is derived from a steel :

- The solidus and liquidus temperature are respectively $T_s = 1696$ K and $T_L = 1740$ K.
- The material model between the solidus and the liquidus is let free to each contributor.
- There are no latent heat exchanges during solid / liquid transformation, and vaporization is not taken into account.
- Thermo-physical properties (λ, ρ, C_p, μ) are constant for each phase (table 1 and 2):

Solid phase $T < 1696$ K	
Density	$\rho = 7500 \text{ kg m}^{-3}$
Specific heat	$C_p = 602 \text{ J K}^{-1} \text{ kg}^{-1}$
Thermal Conductivity	$\lambda = 24 \text{ W m}^{-1} \text{ K}^{-1}$

Table 1: Thermo-physical properties for the solid phase

Liquid phase $T > 1740$ K	
Density	$\rho = 6350 \text{ kg m}^{-3}$
Specific heat	$C_p = 695 \text{ J K}^{-1} \text{ kg}^{-1}$
Thermal Conductivity	$\lambda = 20 \text{ W m}^{-1} \text{ K}^{-1}$
Dynamic viscosity	$\mu = 2,5 \cdot 10^{-3} \text{ kg.m}^{-1} \text{ s}^{-1}$
Dilatation coefficient	$\beta = 10^{-4} \text{ K}^{-1}$

Table 2: Thermo-physical properties for the liquid phase

Boundary conditions

Thermal conditions:

- The heat flux through the top surface is the sum of three terms :

$$\Phi_{\text{top}} = \Phi_{\text{source}} - \Phi_{\text{convection}} - \Phi_{\text{radiation}}$$

- The heat source follows a Gaussian distribution :

$$\varphi_{\text{source}}(r) = \frac{P}{2\pi r_0^2} \exp\left(-\frac{r^2}{2r_0^2}\right)$$

With $r_0 = 3 \cdot 10^{-3}$ m, $P = 900$ W

The radiation exchange (applied on the top surface, including the surface underneath the heat source) is expressed by :

- $\Phi_{\text{radiation}} = \varepsilon \sigma (T^4 - T_0^4)$ with :

σ the Stefan-Boltzmann constant, emissivity $\varepsilon = 0.5$ and $T_0 = 300$ K;

- Convective exchange with the air (also applied on the whole surface)

$$\Phi_{\text{convection}} = h(T - T_0) :$$

with $h = 15 \text{ W m}^{-2} \text{ K}^{-1}$;

- The lateral side is adiabatic
- On the lower side, a Dirichlet condition is set: the temperature decreases linearly from the axis to the part extremity from 800 to 400 K

Momentum conditions:

- Symmetry axis: $u_r = 0$;
- Top side : $u_z = 0$;
- Lower and lateral side : $\vec{u} = \vec{0}$;
- Surface tension: Since the free surface remains flat in our hypothesis, the boundary condition is :

$$\mu \frac{\partial u_r}{\partial z} = \frac{\partial \gamma}{\partial T} \frac{\partial T}{\partial r} \quad (\text{Eq.: 1})$$

Where γ is the surface tension. Its gradient along the tangential direction u_r is balanced by shear stress. In this benchmark two values for the surface tension gradient are treated in order to cover its range of variation as a function of temperature⁴:

- **Case A:** $\frac{\partial \gamma}{\partial T} = -10^{-4} \text{ N m}^{-1} \text{ K}^{-1}$
- **Case B:** $\frac{\partial \gamma}{\partial T} = 10^{-4} \text{ N m}^{-1} \text{ K}^{-1}$

Those selected values of temperature dependence of the surface tension as been chosen moderate in order to be consistent with a laminar flow and to allow a large range of contributors.

Driving forces and governing equations:

For this benchmark, only the surface tension gradient at the weld pool surface and the buoyancy term are taken into account.

The governing equations for the incompressible Newtonian fluid flow and heat transfer in the weld pool are written as follows:

$$\nabla \cdot \vec{\mathbf{u}} = 0,$$

for the mass conservation.

$$\rho \left(\frac{\partial \vec{\mathbf{u}}}{\partial t} + (\nabla \vec{\mathbf{u}}) \vec{\mathbf{u}} \right) = \nabla \cdot \left(-P \mathbf{I} + \mu \left(\nabla \vec{\mathbf{u}} + (\nabla \vec{\mathbf{u}})^T \right) \right) + \vec{\mathbf{F}}_{body} \quad (\text{Eq.: 2})$$

for the momentum conservation. $\vec{\mathbf{F}}_{body}$ represents here buoyancy term in the Boussinesq approximation:

$$\vec{\mathbf{F}}_{body} = \rho_{ref} \left[1 - \beta (T - T_{ref}) \right] \vec{\mathbf{g}}.$$

The energy conservation equation is :

$$\rho C_p \left[\frac{\partial T}{\partial t} + \vec{\mathbf{u}} \cdot \vec{\nabla} T \right] = \vec{\nabla} \cdot (\lambda \vec{\nabla} T)$$

As said above, the material characteristics are taken constant for each phase.

Output observables:

The transient calculation observables are evaluated for the physical instants $t = 1, 2, 3, 4$ and 5 s. For each instant, the outputs are:

- The top side temperature profile ($z = 10$ mm).
- The axial temperature profile ($r = 0$).
- The top side radial velocity component profile v_r ($z = 10$ mm).
- The axial vertical velocity component profile: v_z ($r = 0$).

COMPUTATIONAL TOOLS

This benchmark has been carried out with five CFD codes, described in this section. All of them except one have used a fixed grid method to solve the phase change problem.

Fluent

The benchmark has been carried out with the CFD code Fluent by a team composed of Fluent France and Air Liquide research division.

Problem formulation

The Navier-Stokes and energy equations have been solved using the double precision segregated solver of Fluent, meaning that the governing equations are solved sequentially. In order to take into account problems which involve solid/liquid phase changes, Fluent provides solidification/melting model that uses an enthalpy-porosity formulation allowing the determination of liquid fraction in

the mushy zone (partially solidified zone). In this model and for a non-zero melting latent heat, the enthalpy of the material is the sum of sensible enthalpy and the product of latent heat and the liquid fraction. In order to take into account the decrease of the velocities in the mushy zone, a sink term is added to the momentum equation, function of the liquid fraction and a "mushy zone constant" (the higher this value, the steeper the decrease of the fluid velocity).

Discretization

Spatial discretization is made of quadrilateral elements. An adaptation grid method is used to refine (add) grid elements at each time step where the gradient of liquid fraction is high (solidification front). A first-order upwind scheme has been used for the momentum equation and the SIMPLE algorithm for the pressure-velocity formulation.

A first-order implicit scheme has been used for time discretization.

Computational parameters

Due to the use of the solution-adaptive refinement of the grid, the number of cells in the computational domain increased from 3720 (60x62) to 8079 (resp. 9537) for $t = 5$ s and a negative (resp. positive) surface tension coefficient. The time step was constant at 5×10^{-3} s.

FemLab

The Lorient antenna of the University of Bretagne Sud conducted the calculations with the multiphysics package, FemLab 3.1, an interactive environment allowing to model coupled phenomena based on partial differential equations, developed by Comsol⁽¹⁰⁾.

Problem formulation

The incompressible Navier-Stokes application mode is chosen to solve the momentum balance equations. For the heat transfer problem the convection and conduction application mode is used. To implement the Marangoni effect, the weak form Boundary application mode is employed. In this mode, the equation (Eq.: 1) is implemented using the weak formulation.

To include the effect of phase change on convection, the phase solid is modeled as an extremely viscous liquid ($\mu = 10^5$ kg. $\text{m}^{-1} \cdot \text{s}^{-1}$). An apparent viscosity is then defined with a smoothed switch function that emulates the step of viscosity at the melting temperature. This FEMLAB's built in smoothed Heaviside function (flc2hs) is also used to smooth out the discontinuity of the other material properties due to the phase-change.

Moreover, the considered set of governing equations is written in dimensionless form, using the following references quantities and related scales for time and pressure: $L_{ref} = 10^{-3}$ m for length; $V_{ref} = 1$ $\text{m} \cdot \text{s}^{-1}$ for velocity; $\Delta T_{ref} = T_s - T_0$ for temperature difference.

Discretizations

The time discretization is performed with a Backward Differentiation Formula scheme of 5th order (BDF 5) associated with an adaptive time stepping algorithm. The

maximum time step was set to 10^{-3} s. The absolute and relative tolerance parameters for the ODE solver were respectively 0.001 and 0.01. These parameters determine the limit for the estimated error in each integration step.

The space discretization is based on triangular elements mesh. A quadratic Lagrange interpolation is used for the energy equation, and a Lagrange P1-P2 for the fluid motion. The Marangoni boundary condition is integrated with Lagrange linear interpolation.

Computational parameters

In order to reduce the computation time, the momentum equations are solved only in a reduced region close to the heat source. The size of this domain was a quarter ellipse of 1.2 mm height and 5.5 mm width for the negative gradient of surface tension and 2.5 mm height and 4 mm width for the positive gradient of surface tension. The top boundary was discretized with a minimum size of 0.015 mm and the quarter ellipse with a minimum size of 0.1 mm resulting in about 35000 DoF mesh. The benchmark simulations were completed under 13h00 on a notebook equipped with an Intel Pentium 1,7 GHz (Centrino technology) and 512 Mo DDRam.

Marcus

Numerical and computational features of the Marcus implementation are presented in this section. Marcus is a software developed at the University of Provence (Polytech'Marseille).

Problem formulation

The Navier-Stokes equations are written in the velocity-pressure formulation and they are supplemented with a Darcy-like term to account for the fluid flow in the solidus-liquidus interval (mushy zone). On the other hand an enthalpy form is used for the energy equation, but it exactly coincides with the standard energy equation in the present test cases in which the melting latent heat is set to zero. Moreover, the considered set of governing equations is written in dimensionless form, using the following references quantities and related scales for time and pressure: $L_{ref}=10^{-2}$ m (disc thickness) for length;

$$V_{ref} = \sqrt{\frac{\partial\gamma}{\partial T} \cdot \frac{\Delta T_{ref}}{\rho L_{ref}}} \quad \text{for velocity; } T_{ref}=10^3 \text{ K for}$$

$$\text{temperature difference; } q_{ref} = \frac{L_{ref}}{\lambda \Delta T_{ref}} \text{ for applied heat flux.}$$

A more detailed presentation of the numerical model together with several previously performed comparison exercises in coupled fluid flow and heat transfer problems have been reported in few papers ⁽¹²⁻¹⁴⁾.

Discretizations

The time discretization is performed with a backward Euler scheme (implicit first order finite difference formula) and constant time step. Concerning the space discretization standard Galerkin finite elements have been used resulting in piecewise bi-quadratic approximation for the velocity and temperature fields (Q2 Lagrange finite element), and

piecewise linear approximation but discontinuous for the pressure (Q-1 non nodal finite element). Thank to this particular approximation choice for the pressure together with a penalized formulation of the mass conservation equation, the pressure has been eliminated at the element level by static condensation.

Computational parameters

Both test cases have been performed with the same computational parameters. A constant time step of $t=10^{-3}$ s (physical units), and a mesh made up of 157x157 Q9 finite elements (in the radial and axial directions), resulting in about 100 000 nodes and 300 000 degrees of freedom (velocity and temperature) enabled us to obtain converged results (independent of space and time discretizations). It is noteworthy that this mesh is mainly concentrated in an upper left quarter defined by $[0, 1.2] \times [0.3, 1]$ in the radial and axial directions, in which the element size are $r=7.7 \cdot 10^{-5}$ m and $z=4.5 \cdot 10^{-5}$ m (physical units), respectively.

Cast3M

Cast3M is a product developed by CEA (Nuclear Energy Division). It is general purpose code for solving differential equations by the finite element method ⁽¹⁵⁾.

Problem formulation

The Navier-Stokes (NS) and energy equation are written in dimensional form in the axisymmetric velocity-pressure-temperature formulation. We have used the fact that the physical properties are constant in conjunction with the Boussinesq and incompressible hypothesis. In the Navier-Stokes equation, the liquid-solid transition is modeled by a large jump in the viscosity (e.g. 10^6). No liquid-solid phase change modeling is done in the energy equation.

Discretization

Discretization in time is done with a backward Euler scheme (implicit first-order finite difference formula). The time-step is chosen adaptively so that the maximum relative speed and temperature variation in a time-step does not exceed a prescribed bound (10 % for speed and 1 % for temperature).

Discretization in space is done with quadratic Lagrange elements for the speed and temperature unknowns and linear Lagrange elements for the pressure.

A streamline diffusion approach is adopted for the stable discretization of the convective term of the momentum and energy conservation.

Linearization of the equations is done via an underrelaxed Quasi-Newton incremental approach which decouples the Navier-Stokes and energy part. The two resulting linear systems are solved with a direct solver of LU-type (with a special ordering of the velocity and pressure unknowns for the NS part). The choice of the underrelaxation parameter is of paramount importance due to the large jump in the viscosity: it is done with a heuristic algorithm.

Computational parameters

For both cases, a first computation was performed on a coarse structured mesh to determine approximately the maximal fluid domain dimensions. The fine mesh consists in two parts: a rectangular structured part near the heat source, a triangular (of Delaunay type) part elsewhere.

Thercast

Thercast is a commercial software package for the tree-dimensional finite element modeling of solidification processes⁽¹⁶⁻¹⁹⁾. It is developed by the Centre de Mise en Forme des Matériaux (CEMEF, Materials Processing Centre) of Ecole des Mines de Paris, in Sophia Antipolis and the company Transvalor S.A. In this benchmark exercise, CEMEF has used the two-dimensional version of the software, also named R2SOL, which is developed in collaboration with Ecole des Mines de Nancy (LSG2M). The capacities of the package are diverse: mould filling, multidomain stress-strain analysis, macrosegregations. It also comprises facilities for initial meshing and dynamic remeshing.

Problem formulation

The incompressible Navier-Stokes equations are solved using a velocity-pressure formulation. The energy conservation equation is solved for the enthalpy variable. A large value of the viscosity is used for the material in the solid state (10^4 Pa s), together with a transition in the mushy state, between solidus and liquidus.

Discretizations

For this application, the chosen spatial discretization consists of linear P1/P1 triangular elements (continuous velocity and pressure field) with least squares pressure stabilization and SUPG (Streamline Upwind Petrov-Galerkin) treatment of advection terms. The inertial advection term $(\nabla \mathbf{u})\mathbf{u}$ is partially implicit, writing $(\nabla \mathbf{u})^t \mathbf{u}^{t-\Delta t}$. The mechanical problem which is composed of the momentum conservation and the mass conservation (here simply $\nabla \cdot \mathbf{u} = 0$) is then linear and non-symmetric. It is solved for velocity and pressure nodal unknowns. The dynamic remeshing facilities of the software are used in order to track automatically the evolution of the welding pool. Regarding time discretization, a Euler-backward implicit scheme is used, together with a constant time step. At each time increment, the momentum and energy equations are solved successively, according to a staggered scheme. The linear sets of equations resulting from space and time discretizations are solved using an iterative solver of the PETSc library⁽²⁰⁾.

Computational parameters

The constant time step is chosen equal to 10^{-3} s. The initial mesh is coarse (mesh size 0.8 mm), except in a rectangular box just below the arc (radius 3 mm, depth 1 mm), where the mesh size is prescribed equal to 0.1 mm. Regarding dynamic remeshing, the prescribed mesh size is 0.020 mm

in the molten pool and 0.8 mm in the solid state. In order to follow the evolution of the molten pool, 49 complete remeshings have been done in Case A calculation, and 61 remeshings in Case B. After 5 s (process time) the meshes are composed of 6400 nodes and 12500 elements in Case A (9300 nodes and 18200 elements in Case B). The computational cost associated with remeshings is about 10 % of total CPU time in Case A and 8 % in Case B. The benchmark has been run on a 1.7 GHz Pentium M Centrino processor, with 512 Mb DDR.

BENCHMARK RESULTS

We present results for both A and B cases. Each observable is monitored each second of physical time until $t=5$ s. The graphs are shown in appendix I. For both cases, the melting occurs after the first second of physical time for all simulations. Then, for $t=1$ s, discrepancies between the different approaches are only due to the energy conservation equation resolution. The temperature distributions follow the same evolution as a function of the spatial coordinate; therefore gradients are taken into account the same way by all contributions. Verification that the 900 W heat flux are actually distributed in the part is done, so that, only the radiation loss boundary condition explains discrepancies.

$$\text{Case A: } \frac{\partial \gamma}{\partial T} = -10^{-4} \text{ N m}^{-1} \text{ K}^{-1}$$

Once a liquid zone is established, the five simulations show the same behaviour. Especially for the pool dimensions which are given with less than 0.12 mm discrepancies, which represents less than 4 % at $t=5$ s.

Velocity distributions are obtained with a good agreement on tendencies. However the maximum value is given with about 15 % discrepancies for the axial velocity component.

The radial velocity component, along the surface is a particularly interesting observable to discriminate models.

In this case, the Marangoni boundary condition generates the highest velocity close to the pool border. As regard as a more accurate material model, this situation is here enhanced by a choice of a temperature independent viscosity, which does not increase in this area. For this observable the five contributions agree on the general tendency of the distribution. However, the oscillations close to the pool border depend on the boundary condition imposed to the momentum conservation equation, or its treatment. The different treatments are:

- FemLab: smooth viscosity gap.
- FLUENT sink term which is a function of liquid fraction and a "mushy zone constant".
- Marcus: smoothed viscosity gap and Darcy boundary condition.
- Cast3m: Smoothed viscosity gap and numerical viscosity.
- Thercast: smooth viscosity gap

Code	Elements and discretisation	Schemes
Fluent	Finite Volume method (2D quadrilateral elements) <ul style="list-style-type: none"> • first order upwind 	First order implicit
FemLab	Triangular Finite Element <ul style="list-style-type: none"> • Lagrange P1-P2 (Navier-Stokes) • Lagrange P2 (Energy) • Lagrange linear (Marangoni) 	BDF – 5
Marcus	Quadrilateral Finite Element Q9 <ul style="list-style-type: none"> • Lagrange Q2 (T and V) • Lagrange Q1 (P) 	Euler Implicit
Cast3m	Quadrilateral Finite Element Q9 <ul style="list-style-type: none"> • Lagrange Q2 (T and V) • Lagrange Q1 (P) 	Euler Implicit
Thercast	<ul style="list-style-type: none"> • Triangular Finite Element momentum: stabilized P1/P1 (V and P) • energy: P1 (H and T) 	Euler Implicit

Table 3: CFD codes and discretisation choices

Code	Degrees of freedom	Convergence	Minimum size elements	Time (hours) / RAM
Fluent Air Liquide	30 000	10^{-3} (continuity and momentum) 10^{-6} (energy)	10^{-9} initial ($7.0 \cdot 10^{-11}$)	4:00 (1 Gb)
FemLab	35 000	Weighted Euclidean norm $< 10^{-6}$	$1.5 \cdot 10^{-5}$	13:00 with 512 Mb
Marcus	300 000	10^{-6}	$7.7 \cdot 10^{-5} \times 4.5 \cdot 10^{-5}$	1:30 x 64 processors / 512 Mb
Cast3m	Case A : 33 000	$\frac{\ V_{i+1} - V_i\ }{\ V_{i+1}\ } < 10^{-5}$	$6.2 \cdot 10^{-5} \times 1.0 \cdot 10^{-5}$	3:00 with 1 Gb
	Case B : 30 000		$1.7 \cdot 10^{-5} \times 2.0 \cdot 10^{-5}$	
Thercast	Dynamic remeshing Case A (at 5 s): 19200 (V,P) 6400 (H)	10^{-6}	$2 \cdot 10^{-5}$	1:23
	Case B (at 5 s): 27900 (V,P) 9300 (H)			2:13 512 Mb

Table 4 CFD codes and numerical results

Case	Figures	Time (s)	Observable
A	(a)	1	Surface temperature (K)
	(b)	2	
	(c)	3	
	(d)	4	
	(e)	5	
	(f)	1	Axial temperature (K)
	(g)	2	
	(h)	3	
	(i)	4	
	(j)	5	
	(k)	2	Radial velocity component along the surface (m/s)
	(l)	3	
	(m)	4	
	(n)	5	
(o)	2	Axial velocity component along symmetry axis (m/s)	
(p)	3		
(q)	4		
(r)	5		
B	(I)		1
	(II)	2	
	(III)	3	
	(IV)	4	
	(V)	5	
	(VI)	1	Axial temperature (K)
	(VII)	2	
	(VIII)	3	
	(XIX)	4	
	(X)	5	
	(XI)	2	Radial velocity component along the surface (m/s)
	(XII)	3	
	(XIII)	4	
	(XIV)	5	
	(XV)	2	Axial velocity component along symmetry axis (m/s)
	(XVI)	3	
	(XVII)	4	
	(XVIII)	5	

Table 5 : Legends of the benchmark results presented in appendix.

Case B: $\frac{\partial\gamma}{\partial T} = 10^{-4} \text{ N m}^{-1} \text{ K}^{-1}$

The surface and axial temperature for a negative gradient of surface tension do not represent the same accordance and discrepancies than for the previous case. Since the Marangoni boundary condition generates a motion which tends to deepen the pool and not to extend it, the main uncertainty occurs for the axial velocity along the symmetrical axis. There are less than 12% discrepancies on the pool depth, whereas the pool radius is given by all contributors within 4%.

All contributions present a 2-wells shape which is a stigma of a two rolls flow structure close to the surface.

Case A $\frac{\partial\gamma}{\partial T} = -10^{-4} \text{ N m}^{-1} \text{ K}^{-1}$

CONCLUDING REMARKS

A numerical benchmark for weld pool simulation has been defined by five teams from research laboratories and industrial companies. This benchmark represents a simplified transient 2D-axisymmetrical weld-pool simulation due to a spot torch. The driving forces taken into account are the buoyancy term and the surface tension gradient for which two cases are treated.

The five teams carried out independently the benchmark with commercial and academic CFD codes.

The surface and axial temperature as well as surface and axial velocity profiles are observed for the first 5 seconds.

- Main trends of temperature and velocity distribution are given compatibly with all five simulations.
- From a contribution to another, discrepancies between 4 to 15% are presented on the pool dimensions, which are a relevant observable to evaluate models. The most relevant one is the one related to the driving force. For case A, the pool radius on the surface as to be monitored whereas the temperature on the axis is more revealing for case B.
- Velocity component accuracy will depend on the boundary conditions model for equation (Eq.: 2). Models presented in this paper include a smoothed viscosity gap, a Darcy porosity condition or numerical viscosity.
- For case B, the two wells shape of the vertical velocity on the axis is produced by all five simulations. The 2-rolls structure on the flow at the surface affects this observable. This case reveals itself to present more difficulties for solvers since a null velocity is required on the axis and on the pool border. Moreover, the velocity magnitude is the same order on the surface and on the axis, which is not the case for case A.

APPENDIX I

The legends are the same on all graphs:

.....	U. Bretagne Sud / Femlab
-----	Polytech'Marseille / Marcus
-----	Air Liquide / Fluent
————	CEA / Cast3M
-----	CEMEF / Thercast

Fig. 2: Graphs Legends

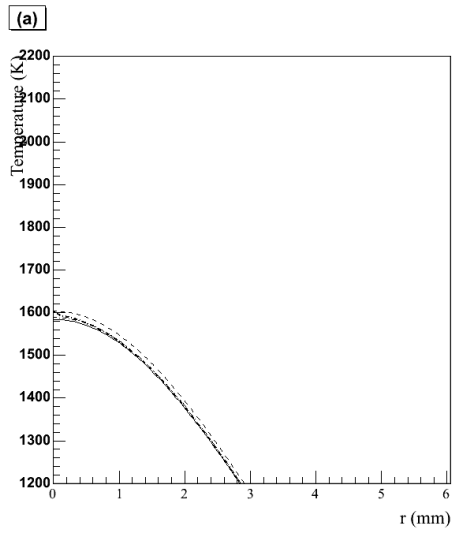


Fig. 3 : Case A - Surface temperature $t = 1$ s

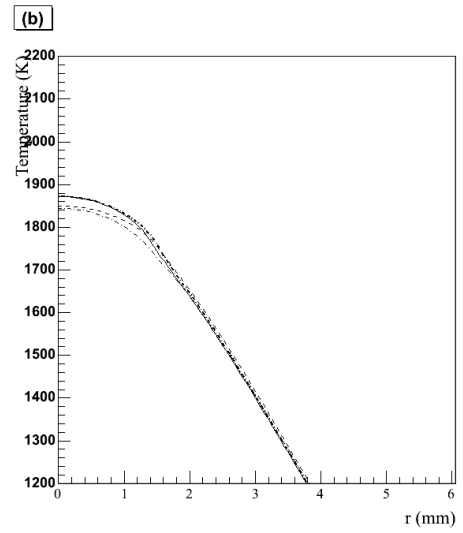


Fig. 4 Case A - Surface temperature $t = 2$ s

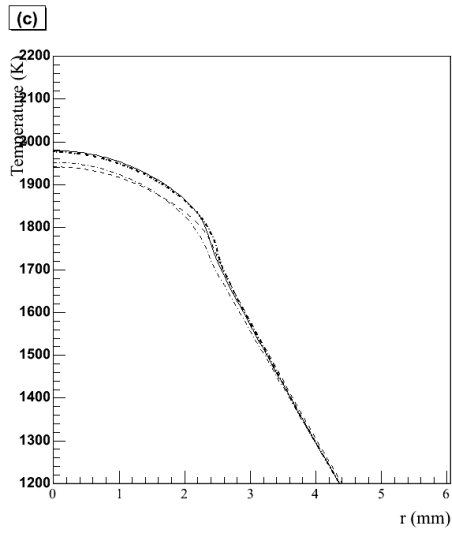


Fig. 5: Case A - Surface temperature $t = 3$ s

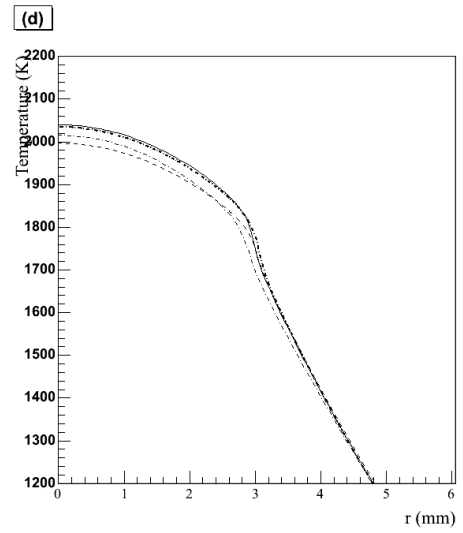


Fig. 6: Case A - Surface temperature $t = 4$ s

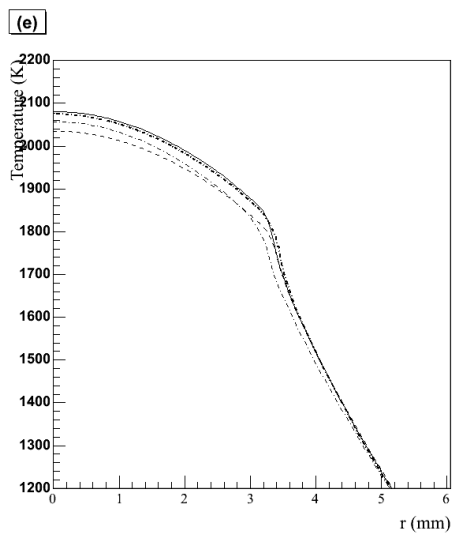


Fig. 7: Case A - Surface temperature $t = 5$ s

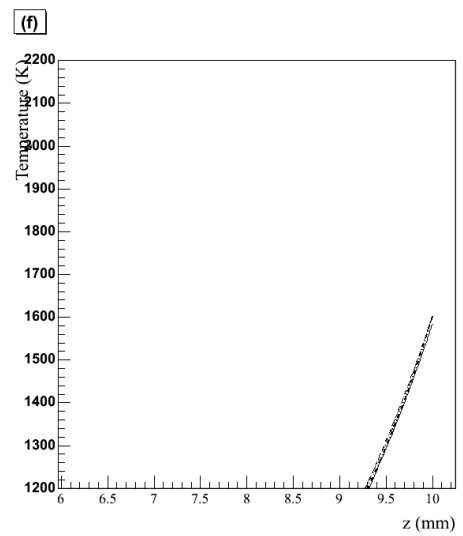


Fig. 8: Case A - Axial temperature $t = 1$ s

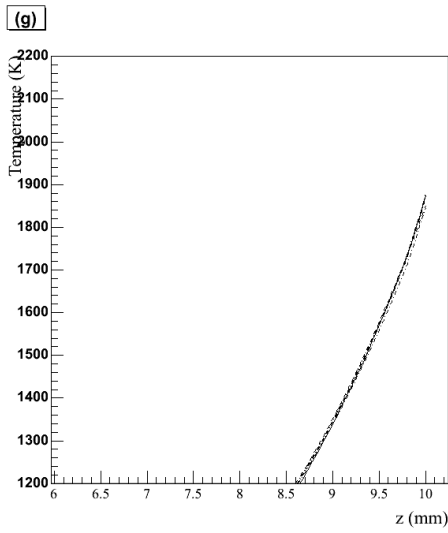


Fig. 9: Case A - Axial temperature $t = 2$ s

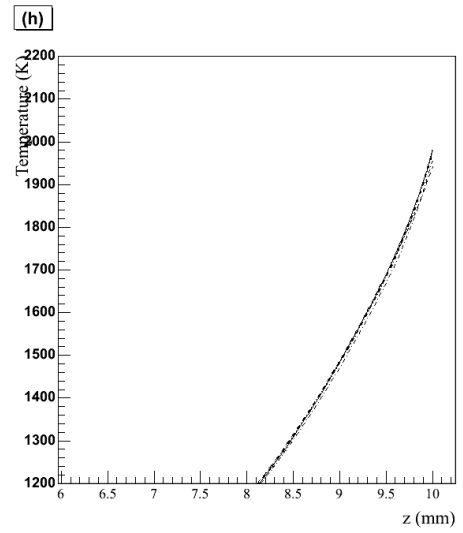


Fig. 10: Case A - Axial temperature $t = 3$ s

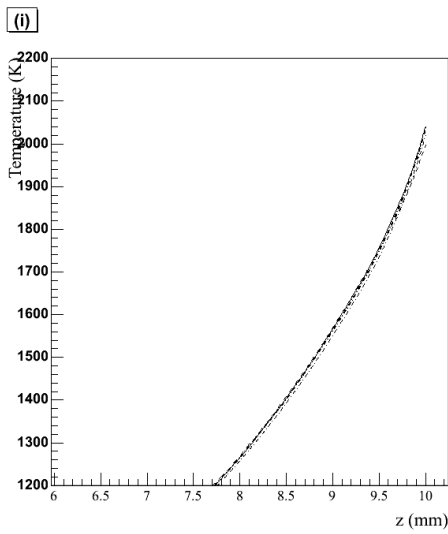


Fig. 11: Case A - Axial temperature $t = 4$ s

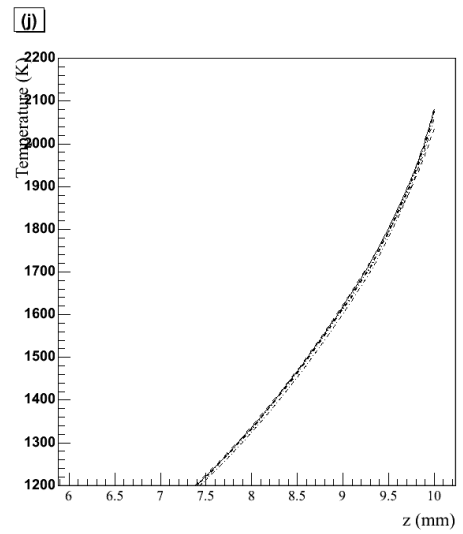


Fig. 12: Case A - Axial temperature $t = 5$ s

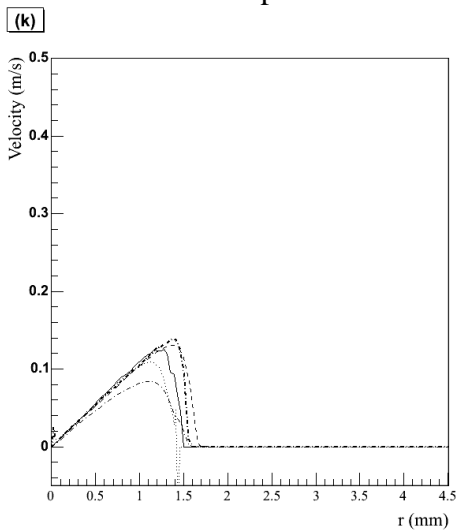


Fig. 13: Case A - Radial velocity component along the surface $t = 2$ s

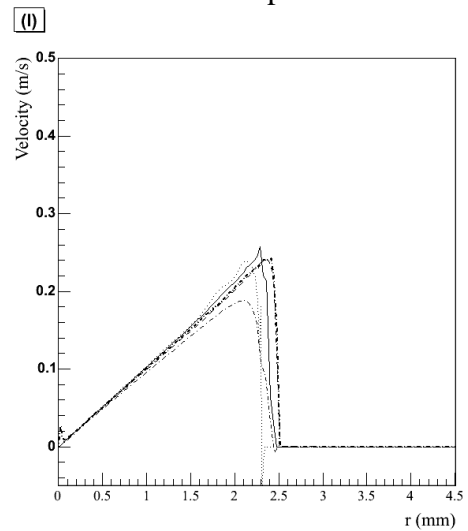


Fig. 14: Case A - Radial velocity component along the surface $t = 3$ s

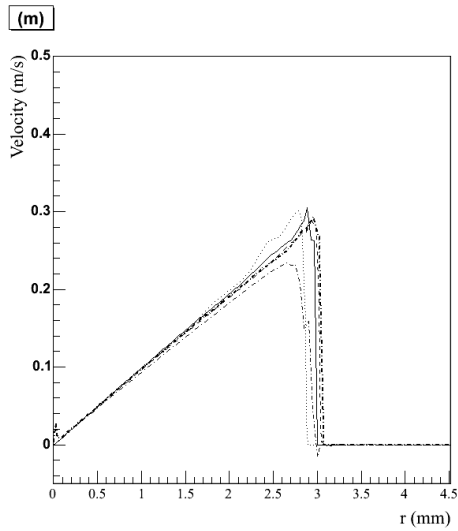


Fig. 15: Case A - Radial velocity component along the surface $t = 4$ s

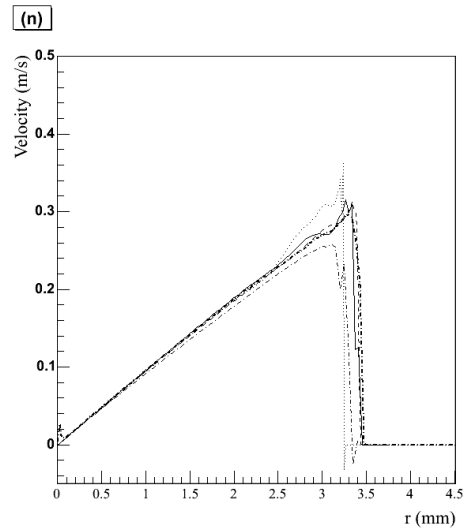


Fig. 16: Case A - Radial velocity component along the surface $t = 5$ s

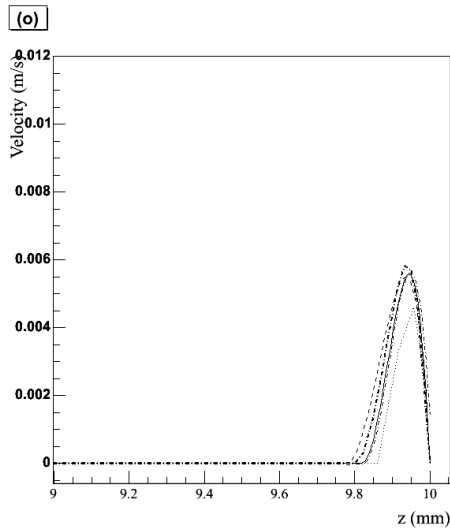


Fig. 17: Case A - Velocity along the symmetrical axis $t = 2$ s

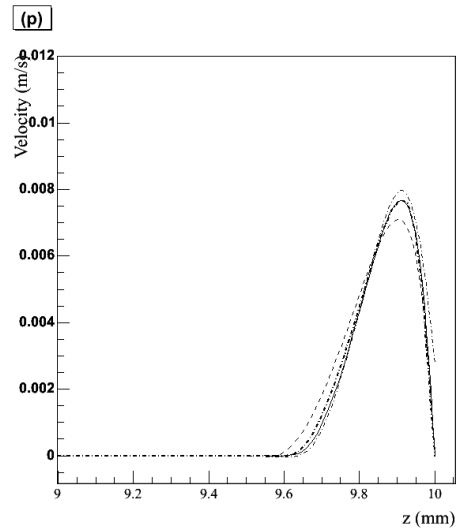


Fig. 18: Case A - Velocity along the symmetrical axis $t = 3$ s

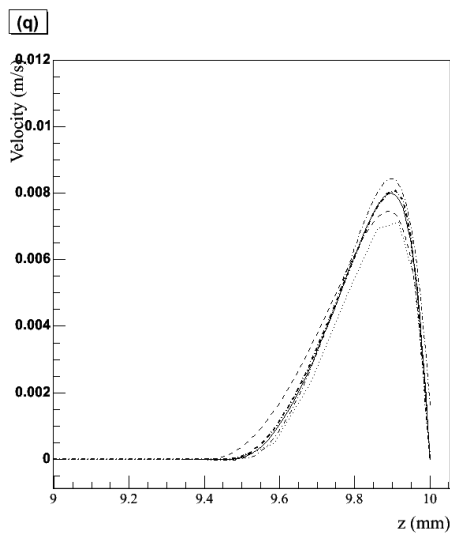


Fig. 19: Case A - Velocity along the symmetrical axis $t = 4$ s

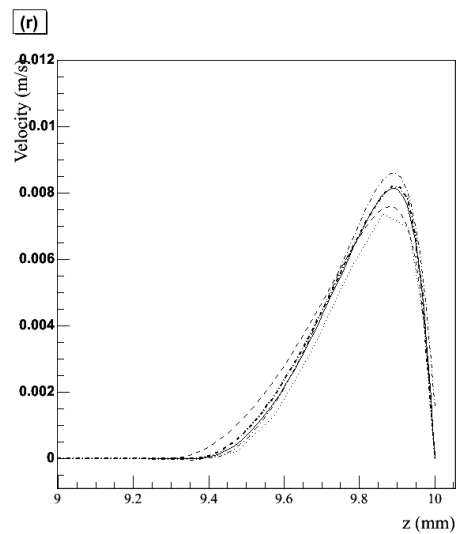


Fig. 20: Case A - Velocity along the symmetrical axis $t = 5$ s

Case B $\frac{\partial \gamma}{\partial T} = 10^{-4} \text{ N m}^{-1} \text{ K}^{-1}$

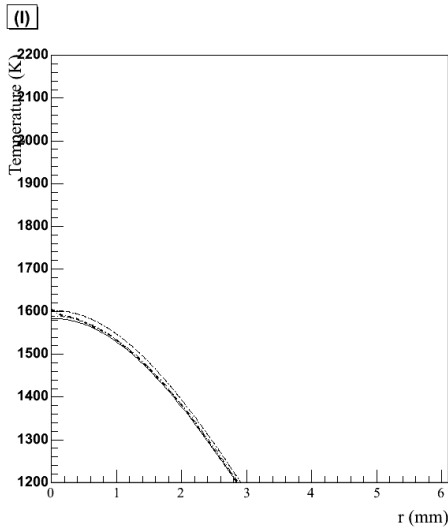


Fig. 21: Case B - Surface temperature t = 1 s

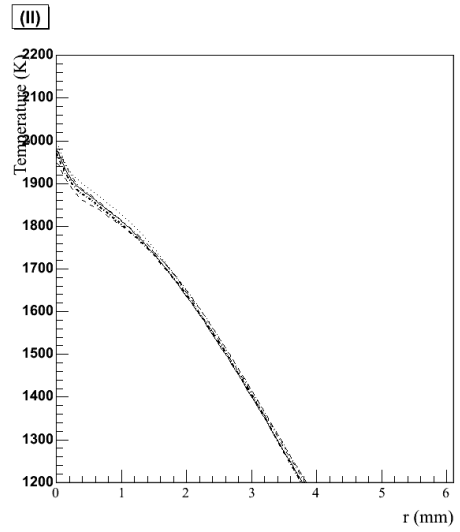


Fig. 22: Case B - Surface temperature t = 2 s

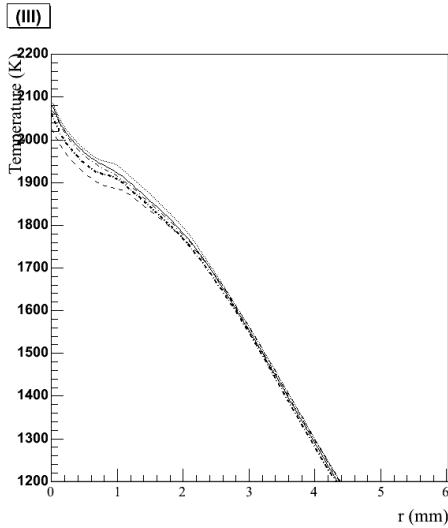


Fig. 23: Case B - Surface temperature t = 3 s

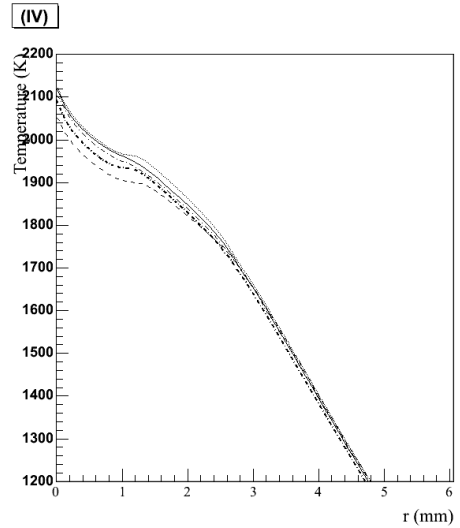


Fig. 24: Case B - Surface temperature t = 4 s

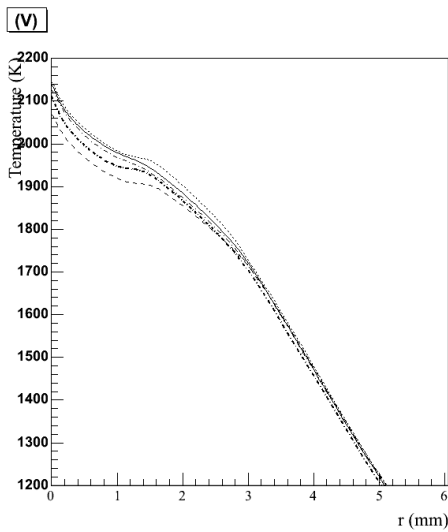


Fig. 25: Case B - Surface temperature t = 5 s

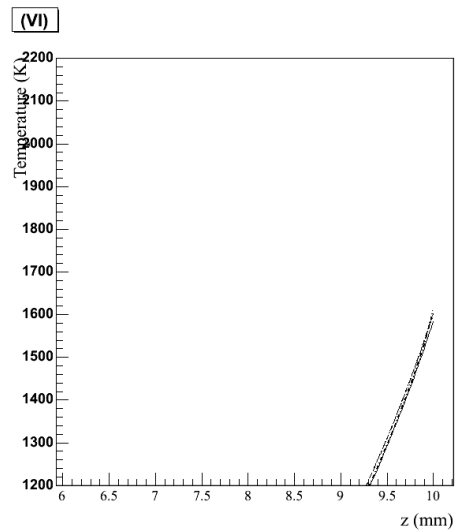


Fig. 26: Case B - Axial temperature t = 1 s

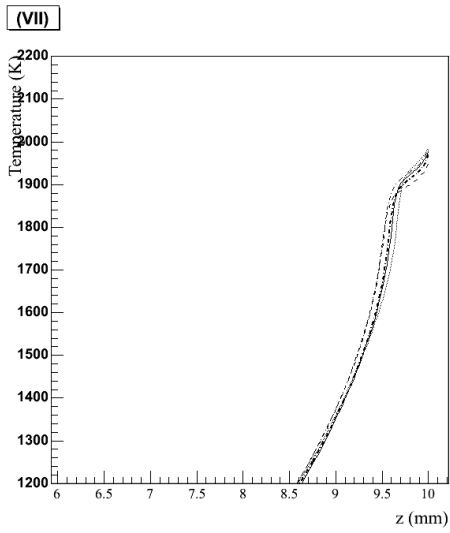


Fig. 27: Case B - Axial temperature $t = 2$ s

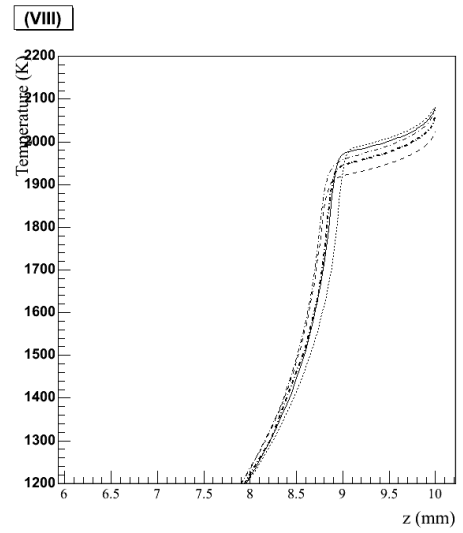


Fig. 28: Case B - Axial temperature $t = 3$ s

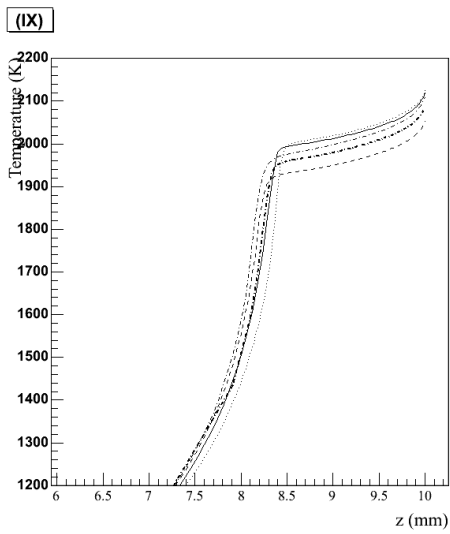


Fig. 29: Case B - Axial temperature $t = 4$ s

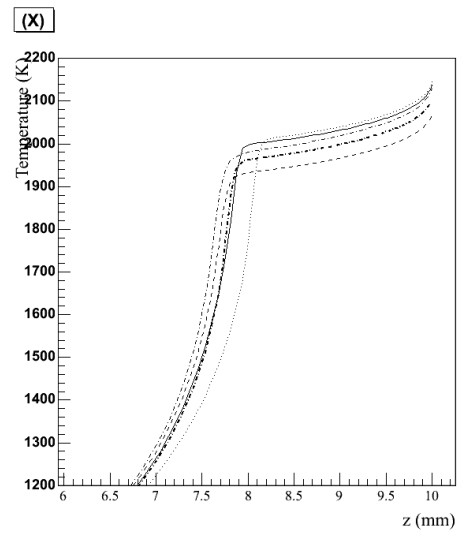


Fig. 30: Case B - Axial temperature $t = 5$ s

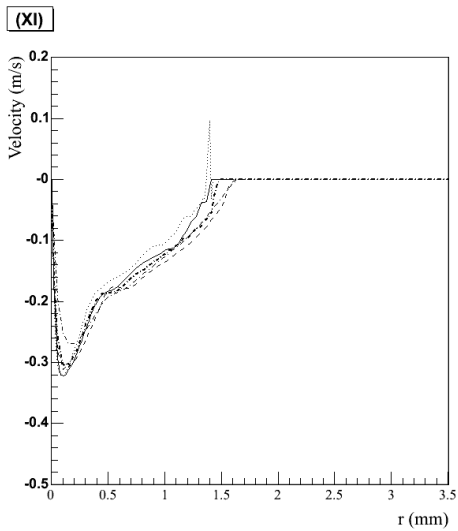


Fig. 31: Case B - Radial velocity component along the surface $t = 2$ s

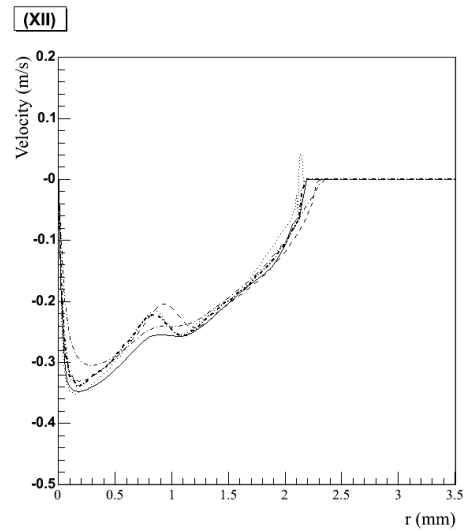


Fig. 32: Case B - Radial velocity component along the surface $t = 3$ s

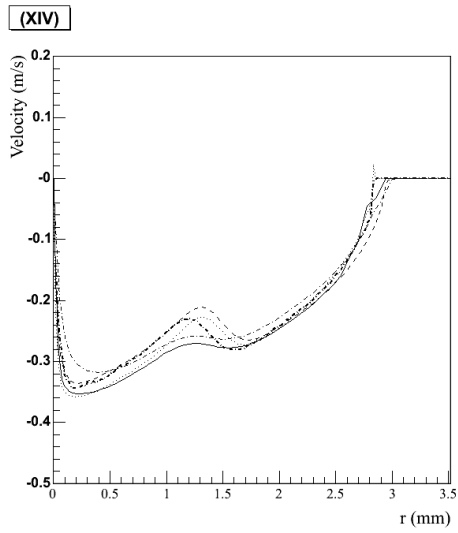


Fig. 33: Case B - Radial velocity component along the surface $t = 4$ s

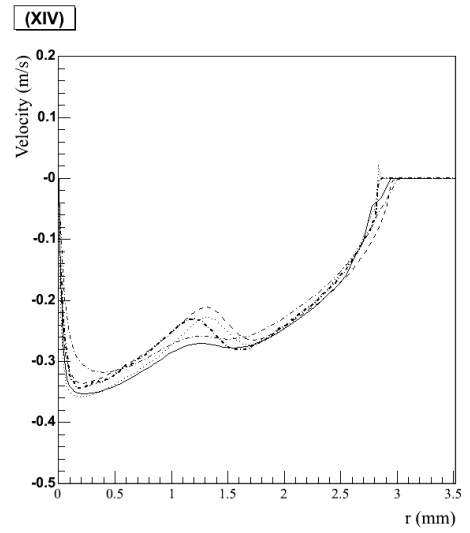


Fig. 34: Case B - Radial velocity component along the surface $t = 5$ s

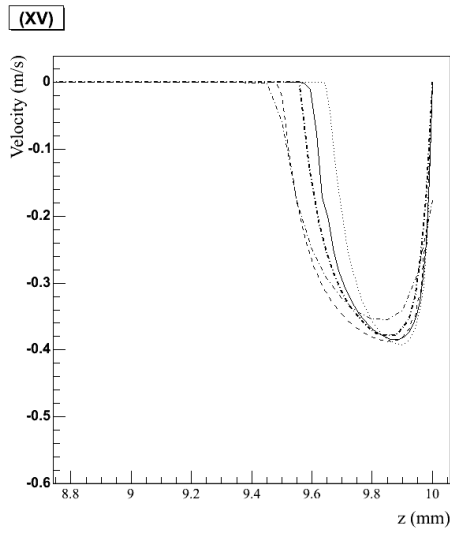


Fig. 35: Case B - Velocity along the symmetrical axis $t = 2$ s

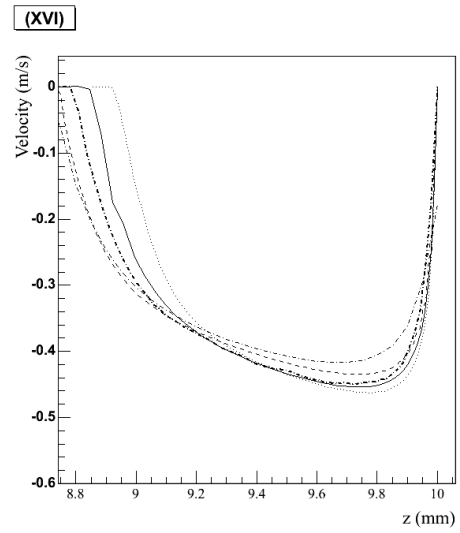


Fig. 36: Case B - Velocity along the symmetrical axis $t = 3$ s

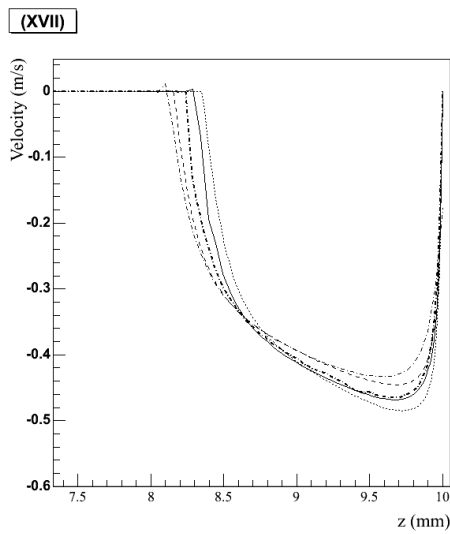


Fig. 37: Case B - Velocity along the symmetrical axis $t = 4$ s

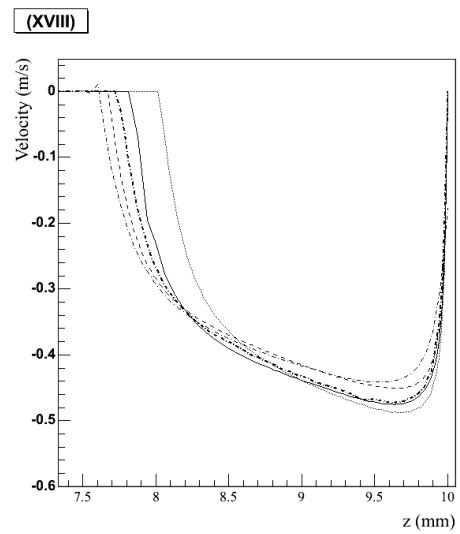


Fig. 38: Case B - Velocity along the symmetrical axis $t = 5$ s

REFERENCES

- 1, G. Oreper and J. Szekely, *J. Fluid Mech.*, **147**, 1984, 53- 79.
- 2, S. Kou and Y.H Wang, *Met. Trans. A.*, **17A** ,1986 , 2271-2277
- 3, T. DebRoy, H. Zhao, W. Wang and G. G. Roy, *Mathematical modelling of weld phenomena*, **6** ,2002, *Conf. Graz 2001*, 21-42
- 4, H.G. Fan, H.L. Tsai, S.J. Na, *Int. J. of Heat and Mass Trans.*, **44** ,2001; 417-428.
- 5, Sindo Kou and D.K. Sun, *Met. Trans. A*, **16A** ,1985, 203-213.
- 6, K. Mundra and T. DebRoy, K.M Kelkar, *Num. Heat. Transfert; Part A*, **29** ,1996, 115-.129
- 7, McKelliget & Szekely *Met. Trans. A*, **17A** ;1986, 1139–1148
- 8, H.G Fan and R. Kovacevic, *J. Phys. D*, **37** (2004), 2331-2544.
- 9, www.fluent.com
- 10, FEMLAB 3.1, user's Guide, 2004 by COMSOL AB (www.comsol.com)
- 11, M. Medale and M. Jaeger, *Int. J. Therm. Sci.*, **38** ,1999, 267-276.
- 12, O. Bertrand, B. Binet, H. Combeau, S. Couturier, Y. Delannoy, D. Gobin, M. Lacroix, P. Le Quere, M. Medale, J. Mencinger, H. Sadat, G. Veira, *Int. J. of Therm. Sci.*, **38**, 1999, 5-26.
- 13, M. Medale, M. Jaeger and A. Kaiss, *Comp. Ass. Mech. Eng. Sci.*, **7**, N°3 2000, 307-320
- 14, M. Medale S. Rabier and C. Xhaard, *Revue Européenne des Eléments finis*, **13** ;2004, 207-229.
- 15, <http://www-cast3m.cea.fr/cast3m/index.jsp>
- 16, www.transvalor.com/ and www.sconconsultants.com/
- 17, M. Bellet, V. D. Fachinotti, *Comput. Methods Appl. Mech. and Engrg.* **193** ;2004, 4355-4381.
- 18, M. Bellet, E. Saez, O. Jaouen, T. Coupez, TMS Annual Meeting, Charlotte (NC, USA), L. Nastac & B. Q. Li (eds.), The Minerals Metals and Materials Society, Warrendale, Pennsylvania, USA ;2004; 209-218.
- 19, M. Bellet, O. Jaouen, I. Poitault, *Int. J. Num. Meth. Heat Fluid Flow* **15** ;2005, 120-142.
- 20, S. Balay, K. Buschelman, W. D. Gropp, D. Kaushik, M. Knepley, L. Curfman McInnes, B.F. Smith, H. Zhang, <http://www.mcs.anl.gov/petsc> , 2001.

This document was created with Win2PDF available at <http://www.win2pdf.com>.
The unregistered version of Win2PDF is for evaluation or non-commercial use only.
This page will not be added after purchasing Win2PDF.